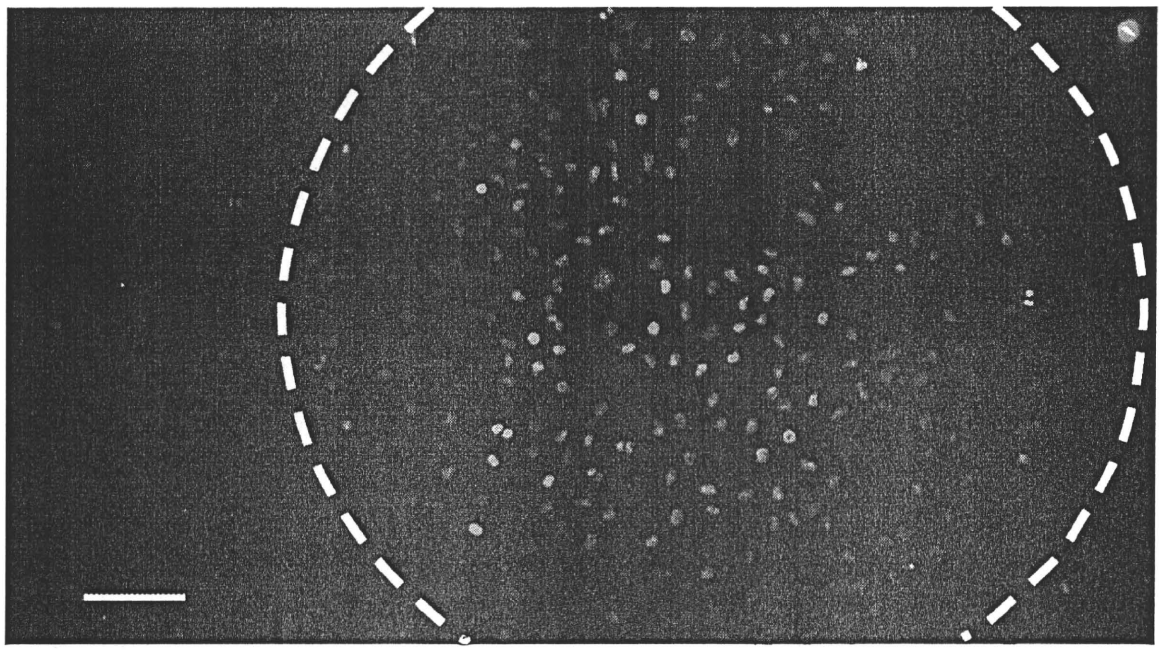

FIG. 4. The irradiated region was identified as γ-H2AX focus-positive cells, which are shown in green. The white dashed line represents the radiation field of the laser plasma X rays. The horizontal and vertical lengths of the radiation field were 850 and 830 μm, respectively. These measurements were 10% of those at the peak absorbed dose obtained from EBT film analysis. Scale bar shows 100 μm.

irradiation experiment was performed at the logarithmic growth phase. Cellular activity is greater than in other phases, and cells proliferate and migrate more actively than under confluent conditions. The dose rate we used is relatively low and the treatment time long (Table 1). In addition, the cells were cultured with collagen type I, which may generate significant cell proliferation and migration under our experimental conditions. Consequently, the cell density may become heterogeneous during irradiation, which accounts for the difference in size between the γ-H2AX focus-positive region and the X-ray spot size.

When the cells were irradiated with 4 MV X rays, similar numbers of foci were observed (Fig. 5D). This suggests that the cells were irradiated with same dose of laser plasma X rays as of 4 MV X rays. Although no significant differences in the number of foci were detected between the cells irradiated with laser plasma X rays and those treated with 4 MV X rays, the number of γ-H2AX foci was approximately double that of phosphorylated ATM foci. Examination of the focus distribution revealed that γ-H2AX foci were expanded around one large phosphorylated ATM foci, especially small γ-H2AX foci, which were not colocalized with other phosphorylated ATM foci (Fig. 6B and C, arrowhead). H2AX was phosphorylated by enzymes other than ATM, such as DNA-dependent protein kinase (DNA-PK) and ataxia telangiectasia and Rad 3-related (ATR) (*25, 26*). These proteins may contribute to the differences between in the numbers of γ-H2AX and phosphorylated ATM foci.

Impact of Dose Rate and Repair Time after Irradiation

H2AX and ATM are phosphorylated immediately after exposure to ionizing radiation, and the activity of these proteins reaches its maximum in a few minutes and then decreases over several hours. In our study, the dose rate of laser plasma X rays is 4.8 cGy/min, which is significantly lower than that of 4 MV X rays. In addition, the time difference from irradiation to fixation between 8 keV laser plasma X rays and 4 MV X rays is approximately 40 min, which makes it difficult to directly compare the effects of 8 keV laser plasma X rays with those of 4 MV X rays on the same time scale (*27, 28*). Thus the transitory changes in γ-H2AX and phosphorylated ATM foci after irradiation, the difference in the dose rates for 8 keV laser plasma X rays and 4 MV X rays and the repair time after irradiation should all be taken into account. The effects of relatively low-dose-rate radiation have been investigated both clinically and biologically. A dose rate ranging from 2 to 12 Gy per hour was defined by ICRU as a medium dose rate (*29*), so the dose rate we used can also be categorized as medium. Medium-dose-rate irradiation is used for brachytherapy for cervical cancer (*30–33*). Tanaka *et al.* reported that no statistically significant differences in therapeutic outcome could be detected between high and medium dose rates (*34*). The biological effectiveness of *in vitro* low-dose-rate radiation has been reported by several researchers using dose rates of a few cGy per hour (*35–40*). Cells irradiated with a low dose rate of ionizing radiation have significantly less γ-H2AX and

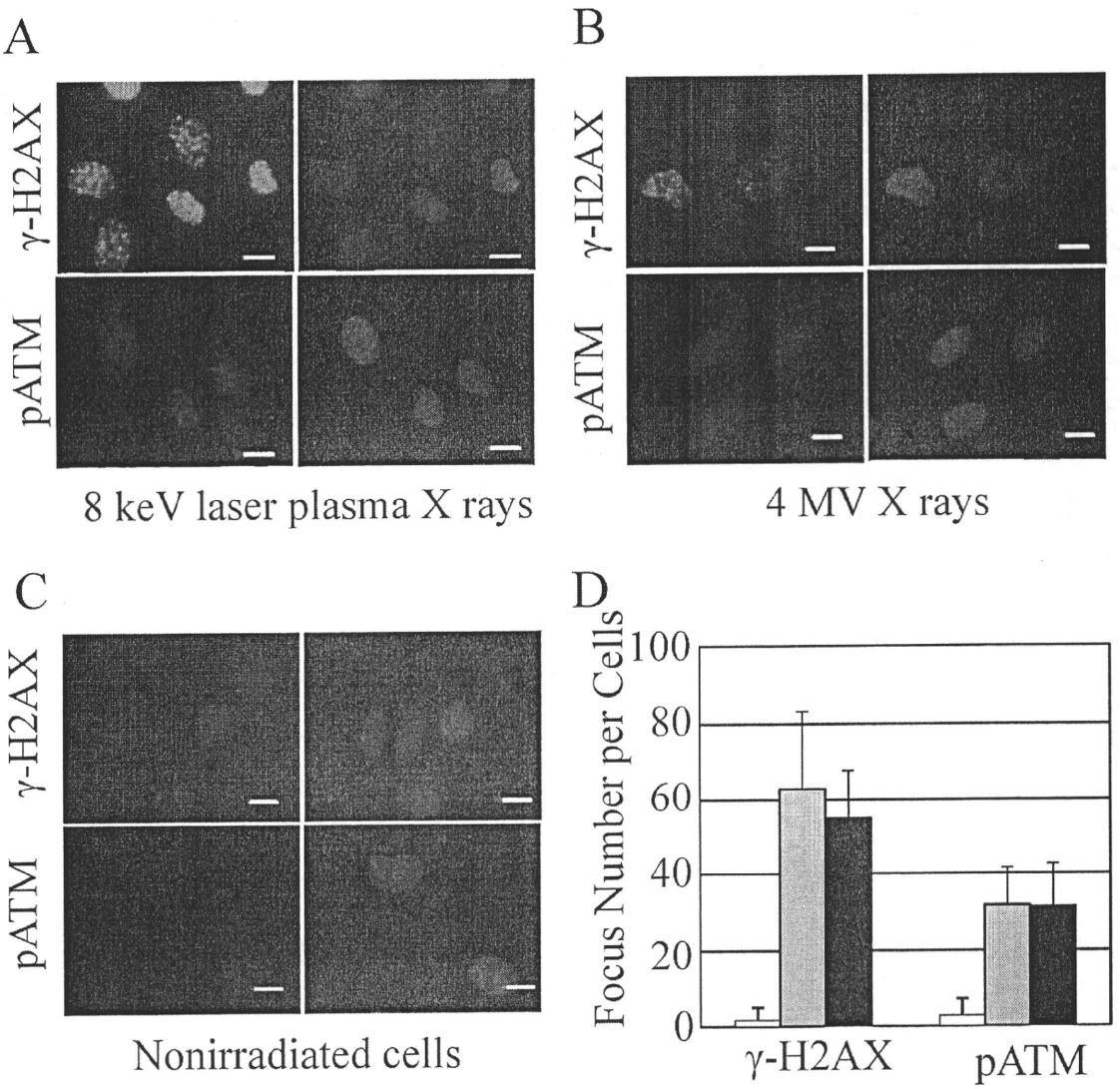

FIG. 5. γ-H2AX and phosphorylated ATM (p-ATM) focus formation after laser plasma X or 4 MV X irradiation. Cells were irradiated with laser plasma X rays (panel A) or 4 MV X rays (panel B) or were not irradiated (panel C). Green, red and blue show the γ-H2AX and p-ATM foci and the nucleus, respectively. Panel D. Number of foci. Gray and black bars represent irradiation with 4 MV and 8 keV laser plasma X rays, respectively. The error bars show standard deviations. No significant differences were detected for either γ-H2AX or p-ATM focus formation (Student's t test, $P = 0.471$ and 0.912 for γ-H2AX and p-ATM, respectively).

phosphorylated ATM focus formation than after high-dose-rate irradiation (*40*). However, the dose rate of laser plasma X rays we used was much higher than used in those studies. Our results also demonstrate that the dose rate and repair time after irradiation are distinct and that repair time was more important for the transitory changes in γ-H2AX and phosphorylated ATM focus formation (Supplementary Fig. 1). The results described above explain why effects such as the dose-rate effect or inverse dose-rate effect were not observed in γ-H2AX and phosphorylated ATM focus formation after laser plasma X irradiation. The effects of laser plasma X rays on DSB induction can therefore be compared to those of 4 MV X rays to determine whether laser plasma X rays can induce DSBs as well as 4 MV X rays. However, cell survival measured by a colony formation assay for 8 keV laser plasma X rays could not be compared with that for 4 MV X rays because a marked dose-rate effect on cell survival occurs and must be considered for such comparisons.

Dosimetry of the Laser Plasma X Rays

The absorbed dose of low-energy X rays such as 8 keV is difficult to measure because low-energy X rays are easily absorbed by air and there are no dosimeters that can measure the absorbed dose accurately. However, Cai *et al.* demonstrated that the absorbed dose of 1.5 keV ultrasoft X rays could be estimated from changes in film density (*41*). In addition, Fletcher *et al.* reported that the percentages of depth dose (PDD) for a range of 50–100 keV X rays measured with EBT film showed good

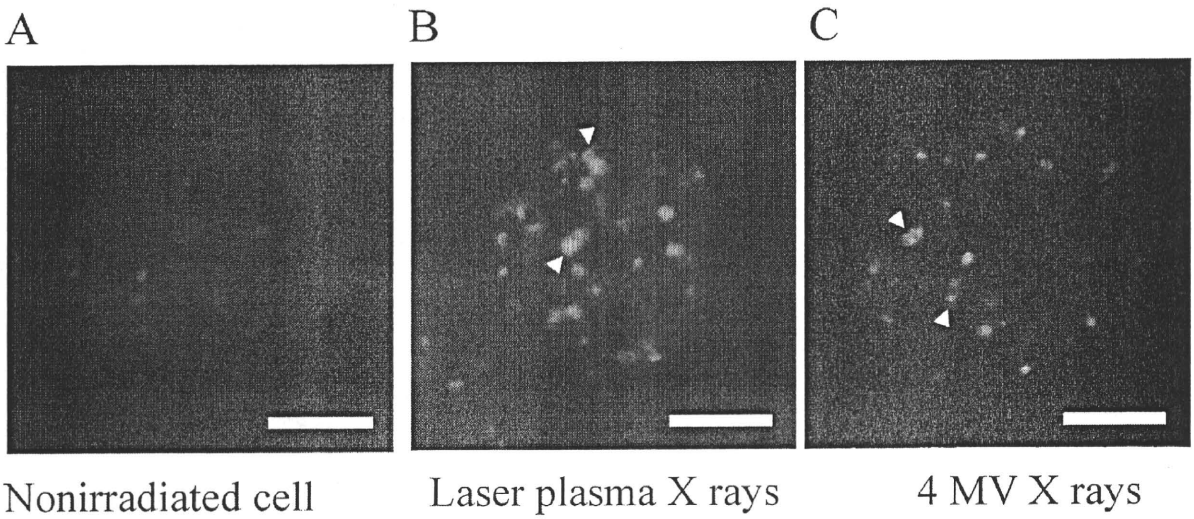

FIG. 6. Colocalization of γ-H2AX and phosphorylated ATM (p-ATM) foci, shown in green and red, respectively. Panels A, B and C show the nonirradiated control, the cells irradiated with laser plasma X rays, and those irradiated with 4 MV X rays, respectively. In both irradiated cases, many small γ-H2AX foci were localized around the one p-ATM (white arrowhead). Scale bar shows 5 μm.

agreement with PDD calculated by Monte Carlo simulation (*42*). These findings indicate that an increase in EBT film density corresponds to the net absorbed dose of low-energy X rays. We therefore adopted densitometry of EBT film to estimate the net absorbed dose of 8 keV laser plasma X rays. A comparison with the results of Cai and Fletcher indicates that we measured the absorbed dose of 8 keV laser plasma X rays accurately in our study. In addition, when cells were irradiated with 2 Gy of 4 MV X rays, which is equivalent to the absorbed dose of 8 keV laser plasma X rays measured by densitometry of EBT film, comparable numbers of γ-H2AX and phosphorylated ATM foci were counted. These findings thus demonstrate the absorbed dose of laser plasma X rays in the target region.

Improvement of Laser Plasma X-Ray System

Since cells are exposed to the laser plasma X rays within sub-picoseconds to picoseconds, it is possible to investigate the involvement of physical and chemical processes (*43, 44*) in radiation responses. For example, the biological responses induced within sub-picoseconds correspond to the formation of the track structure after particle-beam irradiation. However, no investigation has been conducted of molecular biological responses brought about by the differences in energy deposition of ionizing radiation within physical and chemical processes. Moreover, a radiation biological study using laser plasma X rays may provide information that is valuable for radiation protection and radiation therapy. Before we can proceed with our research, the stability of the laser plasma X-ray system must be improved. As shown in Table 1, the dose rate of the laser plasma X rays was relatively low and changed considerably throughout the experiment. Moreover, the system is highly dependent on laser conditions such as laser intensity, alignment of the X-ray focusing devices, and debris production. Debris is the most critical problem for maintaining the stability of the dose rate and uniformity of treatment. The debris is composed of grains of the target material and is produced by target ablation corresponding to the laser plasma X-ray generation. The debris gradually accumulates on the laser pass and optical devices with every irradiation and thus impairs laser reflection and transmission. To overcome this problem, a debris filter must be installed on the optical device. Moreover, the nonuniformity of the irradiation field, which is due to variations in distribution of X-ray intensity, must be also improved. For laser plasma X irradiation, a polycapillary X-ray lens was adopted, so that the X-ray intensity was determined by the Gaussian distribution (Fig. 2B). However, this problem can be solved easily by using a pinhole mask. This is the most effective solution for the nonuniform field. The selectivity of the X-ray energy and dose rate must also be improved for an effective investigation of the fundamental processes involved in radiation biology. The energy of laser plasma X rays can easily be selected by using a solid target. Moreover, the dose rate can be increased by improving the X-ray conversion efficiency and reducing the size of the X-ray spot. Further research is in progress into the relationship between the fundamental processes of radiation biology and molecular biological responses resulting after X irradiation.

SUPPLEMENTARY INFORMATION

Supplementary Fig. 1. Time course of γ-H2AX and phosphorylated ATM (p-ATM) foci. The cells were

irradiated with 2 Gy of 4 MV X rays and then incubated for the indicated times. Then the cells were fixed and stained with primary and secondary antibodies as described in the Materials and Methods. Panel A: Images of γ-H2AX and p-ATM foci. Scale bar shows 5 μm. Panel B: Number of γ-H2AX and p-ATM foci. White, gray and meshed bars show the nonirradiated cells and the cells 30 min and 90 min after irradiation, respectively. The values were obtained from three independent experiments. After 90 min irradiation, the number of γ-H2AX and p-ATM foci had been significantly reduced compared with the number 30 min after irradiation (Student's t test, $P < 0.001$). http://dx.doi.org/10.1667/RR2178.1.S1

ACKNOWLEDGMENTS

We are indebted to Nariaki Matsuura, M.D., Professor of the Laboratory of Molecular Pathology, Osaka University Graduate School of Medicine and Health Science, Osaka, Japan, for his helpful discussions and technical support. This work was performed in part under the auspices of the "Mono-energetic quantum beamscience with petawatt lasers" project supported by the Japan Ministry of Education, Culture, Sports, Science and Technology (MEXT), and of the "Influence of radiation therapy on cancer invasion, metastasis and angiogenesis" project supported by a Grant-in-Aid for Scientific Research from the Japan Society for Promotion of Science (No. 08041858).

Received: February 16, 2010; accepted: June 9, 2010; published online: August 18, 2010

REFERENCES

1. T. Guo, C. Spielmann, B. C. Walker and C. P. J. Barty, Generation of hard x rays by ultrafast terawatt lasers. *Rev. Sci. Instrum.* **22**, 41–47 (2001).
2. H. Yamada, H. Murakami and Y. Shimada, Cu Kα pulse generation in an X-ray tube with a plasma cathode induced by a femtosecond laser pulse. *Radiat. Phys. Chem.* **78**, 375–379 (2009).
3. Y. Okano, Y. Hironaka, K. G. Nakamura and K. Kondo, Energy distribution of electrons ejected from a copper target in a femtosecond laser field of 10^{17} W/cm^2. *J. Appl. Phys.* **95**, 2278–2282 (2004).
4. M. Folkard, G. Schettino, B. Vojnovic, S. Gilchrist, A. G. Michette, S. J. Pfauntsch, K. M. Prise and B. D. Michael, A focused ultrasoft X-ray microbeam for targeting cells individually with submicrometer accuracy. *Radiat. Res.* **156**, 796–804 (2001).
5. T. Sun and D. Xunliang, Study on the measurement of properties of polycapillary X-ray lens. *Nucl. Instrum. Methods Phys. Res. B* **226**, 651–658 (2004).
6. I. V. Tomov, J. Chen, X. Ding and P. M. Rentzepis, Efficient focusing of hard X-rays generated by femtosecond laser driven plasma. *Chem. Phys. Lett.* **389**, 363–366 (2004).
7. C. Reich, P. Gibbon, I. Uschmann and E. Förester, Yield of optimization and time structure of femtosecond laser plasma Kα sources. *Phys. Rev. Lett.* **84**, 4846–4849 (2000).
8. A. Krol, A. Ikhlef, J. C. Kieffer, D. A. Bassano, C. C. Chamberlain, Z. Jiang, H. Pépin and S. C. Prasad, Laser-based microfocused X-ray source for mammography: feasibility study. *Med. Phys.* **24**, 725–732 (1997).
9. J. M. Rajyaguru, M. Kado, K. Nekula, M. C. Richardson and M. J. Muszynski, High resolution X-ray micrography of live Candida albicans using laser plasma pulsed point X-ray sources. *Microbiology* **143**, 733–738 (1997).
10. J. M. Rajyaguru, M. Kado, M. C. Richardson and M. J. Muszynski, X-ray micrography and imaging of Escherichia coli cell shape using laser plasma pulsed point X-ray sources. *Biophys. J.* **72**, 1521–1526 (1997).
11. M. Kado, M. C. Richardson, J. M. Rajyaguru, M. Muszunski, H. Friedman and Y. Yamamoto, Direct ultrastructural imaging of macrophages using a novel X-ray contact microscopy. *Proc. Soc. Exp. Biol. Med.* **220**, 27–30 (1990).
12. B. C. Ferreira, M. C. Lopes and M. Capela, Evaluation of an Epson flatbed scanner to read Gafchromic EBT films for radiation dosimetry. *Phys. Med. Biol.* **54**, 1073–1085 (2009).
13. A. Niroomand-Rad, C. R. Blackwell, B. M. Coursey, K. P. Gall, J. M. Galvin, W. L. Mclauvhlin, A. S. Meigooni, R. Nath, J. E. Rodgers and C. G. Soares, Radiochromic film dosimetry: recommendations of AAPM Radiation Therapy Committee Task Group 55. American Association of Physicists in Medicine. *Med. Phys.* **25**, 2093–2115 (1998).
14. C. G. Sorges, Radiochromic film dosimetry. *Radiat. Meas.* **41**, S100–S116 (2007).
15. E. E. Wilcox, G. M. Daskalov, G. Pavlonnis 3rd, R. Shumway, B. Kaplan and, E. VanRooy, Dosimetric verification of intensity modulated radiation therapy of 172 patients treated for various disease sites: comparison of EBT film dosimetry, ion chamber measurements, and independent MU calculations. *Med. Dosimetry* **33**, 303–309 (2008).
16. E. E. Wilcox and G. M. Daskalov, Evaluation of GAFCHROMIC EBT film for Cyberknife dosimetry. *Med. Phys.* **34**, 1967–1974 (2007).
17. G. Coscia, E. Vaccara, R. Corvisiero, P, Cavazzani, F. G. Ruggieri and G. Taccini, Fractionated stereotactic radiotherapy: a method to evaluate geometric and dosimetric uncertainties using radiochromic films. *Med. Phys.* **36**, 2870–2880 (2009).
18. C. J. Bakkenist and M. B. Kastan, DNA damage activates ATM through intermolecular autophosphorylation and dimer dissociation. *Nature* **421**, 499–506 (2003).
19. S. Bruma, B. P. Chen, M. Murphy, A. Kurimasa and D. J. Chen, ATM phosphorylates histone H2AX in response to DNA double-strand breaks. *J. Biol. Chem.* **276**, 42462–4247 (2001).
20. E. P. Rogakou, D. R. Pilch, A. H. Orr, V. S. Ivanova and W. M. Bonner, DNA double-stranded breaks induce histone H2AX phosphorylation on serine 139. *J. Biol. Chem.* **273**, 5858–5868 (1998).
21. R. Shroff, A. Arbel-Eden, D. Pilch, G. Ira, W. M. Bonner, J. H. Petrini, J. E. Haber and M. Lichten, Distribution and dynamics of chromatin modification induced by a defined DNA double-strand break. *Curr. Biol.* **14**, 1703–1711 (2004).
22. C. Tillman, G. Grafström, A. C. Jonsson, B. A. Jönsson, I. Mercer, S. Mattsson, S. E. Strand and S. Svanberg, Survival of mammalian cells exposed to ultrahigh dose rates from a laser-produced plasma X-ray source. *Radiology* **213**, 860–865 (1999).
23. K. Shinohara, H. Nakano, N. Miyazaki, M. Tago and R. Komada, Effects of single-pulse (< or = 1 ps) X-rays from laser-produced plasmas on mammalian cells. *J. Radiat. Res.* **45**, 509–514 (2004).
24. R. I. Freshney, *Culture of Animal Cells. A Manual of Basic Technique*, 5th ed., pp. 351–352. Wiley-Liss, New York, 2005.
25. J. An, Y. C. Huang, O. Z. Xu, L. J. Zhou, Z. F. Shang, B. Huang, Y. Wang, X. D. Liu, D. C. Wu and P. K. Zhou, DNA-PKcs plays a dominant role in the regulation of H2AX phosphorylation in response to DNA damage and cell cycle progression. *BMC Mol. Biol.* **11**, 18 (2010).
26. J. D. Friesner, B. Liu, K. Culligan and A. B. Britt, Ionizing radiation-dependent γ-H2AX focus formation requires ataxia telangiectasia mutated and ataxia telangiectasia mutated and Rad3-related. *Mol. Biol. Cell* **16**, 2566–2576 (2005).
27. S. V. Costes, A. Boissière, S. Ravani, R. Romano, B. Parvin and M. H. Barcellos-Hoff, Imaging features that discriminate between foci induced by high- and low-LET radiation in human fibroblasts. *Radiat. Res.* **165**, 505–516 (2006).

28. K. Suzuki, H. Okada, M. Yamauchi, Y. Oka, S. Kodama and M. Watanabe, Qualitative and quantitative analysis of phosphorylated ATM foci induced by low-dose ionizing radiation. *Radiat. Res.* **165**, 499–504 (2006).
29. ICRU, *Dose and Volume. Specifications for Reporting Intracavitary Therapy in Gynecology*. Report 38, International Commission on Radiation Units and Measurements, Bethesda, MD, 1985.
30. M. N. Andrieu, H. Edinsel and C. Kurtman, Early results of exclusive radiotherapy in advanced stages cervical carcinoma performed with reference to ICRU Report 38. *Radiat. Med.* **19**, 255–261 (2001).
31. F. Leborgne, J. F. Fowler, J. H. Leborgne, E. Zubizarreta and R. Chappell, Fractionation in medium dose rate brachytherapy of cancer of the cervix. *Int. J. Radiat. Oncol. Biol. Phys.* **35**, 907–914 (1996).
32. F. Leborgne, J. F. Fowler, J. H. Leborgne, E. Zubizarreta and R. Chappell, Biologically effective doses in medium dose rate brachytherapy of cancer of cervix. *Radiat. Oncol. Investig.* **5**, 289–299 (1997).
33. F. Leborgne, J. F. Fowler, J. H. Leborgne, E. Zubizarreta and R. Curochquin, Medium-dose-rate brachytherapy of cancer of the cervix: Preliminary results of a prospectively designed schedule based on the linear-quadratic model. *Int. J. Radiat. Oncol. Biol. Phys.* **45**, 1061–1064 (1991).
34. E. Tanaka, O. Ryoong-jin, Y. Yamada, H. Shiomi, S. Shimamoto, T. Teshima, T. Inoue and T. Inoue, Prospective study of HDR (^{192}Ir) versus MDR (^{137}Cs) intracavitary brachytherapy for carcinoma of the uterine cervix. *Brachytherapy* **2**, 85–90 (2003).
35. B. Marples and S. J. Collis, Low-dose hyper-radiosensitivity: past, present, and future. *Int. J. Radiat. Oncol. Biol. Phys.* **70**, 1310–1218 (2007).
36. M. C. Joiner, B. Marples, P. Lambin, S. C. Short and I. Turesson, Low-dose hypersensitivity: current status and possible mechanisms. *Int. J. Radiat. Oncol. Biol. Phys.* **49**, 379–89 (2001).
37. H. Nakamura, Y. Yasui, N. Saito, A. Tashibana, K. Komatsu and K. Ishizaki, DNA repair defect in AT cells and their hypersensitivity to low-dose-rate radiation. *Radiat. Res.* **165**, 277–282 (2006).
38. T. A. Kato, H. Nagasawa, M. M. Weil, J. B. Little and J. S. Bedford, Levels of γ-H2AX foci after low-dose-rate irradiation reveal a DNA DSB rejoining defect in cells from human ATM heterozygotes in two AT families and in another apparently normal individual. *Radiat. Res.* **166**, 443–453 (2006).
39. L. Enns, K. T. Bogen, J. Wizniak, A. D. Murtha and M. Weinfeld, Low-dose radiation hypersensitivity is associated with p53-dependent apoptosis. *Mol. Cancer. Res.* **2**, 557–566 (2004).
40. S. J. Collis, J. M. Schwaninger, A. J. Ntambi, T. W. Keller, W. G. Nelson, L. E. Dillehay and T. L. DeWeese, Evasion of early cellular response mechanisms following low level radiation-induced DNA damage. *J. Biol. Chem.* **26**, 49624–49632 (2004).
41. Z. Cai, X. Pan, D. Hunting, P. Cloutier, R. Lemay and L. Sanche, Dosimetry of ultrasoft X-rays (1.5 keV $Al_{K\alpha}$ using radiochromatic films and colour scanners. *Phys. Med. Biol.* **48**, 4111–4124 (2003).
42. C. L. Fletcher and J. A. Mills, An assessment of GafChromic film for measuring 50 kV and 100 kV percentage depth dose curves. *Phys. Med. Biol.* **53**, N209–N218 (2008).
43. A. Migus, Y. Gauduel, J. L. Martin and A. Antonetti, Excess electrons in liquid water: First evidence of a prehydrated state with femtosecond lifetime. *Phys. Rev. Lett.* **58**, 1559–1562 (1987).
44. F. H. Long, H. Lu and K. B. Eisenthal, Femtosecond studies of the presolved electron: An excited state of the solvated electrons? *Phys. Rev. Lett.* **64**, 1469–1472 (1990).

A comparison of the respiratory signals acquired by different respiratory monitoring systems used in respiratory gated radiotherapy

Yuki Otani[a)]
Department of Medical Physics and Engineering, Osaka University Graduate School of Medicine, Osaka 565-0871, Japan

Ichirou Fukuda, Nobuhiro Tsukamoto, Yu Kumazaki, and Hiroshi Sekine
Department of Radiation Oncology, Saitama Medical University, Saitama 350-1298, Japan

Etsuko Imabayashi
Department of Nuclear Medicine, Saitama Medical University, Saitama 350-1298, Japan

Osamu Kawaguchi
Department of Radiology, Keio University, Tokyo 160-8582, Japan

Takayuki Nose
Department of Radiation Oncology, Nippon Medical School Tama Nagayama Hospital, Tokyo 206-8512, Japan

Teruki Teshima
Department of Medical Physics and Engineering, Osaka University Graduate School of Medicine, Osaka 565-0871, Japan

Takushi Dokiya
Department of Radiation Oncology, Saitama Medical University, Saitama 350-1298, Japan

(Received 12 March 2010; revised 15 October 2010; accepted for publication 18 October 2010; published 8 November 2010)

Purpose: Respiratory monitoring systems are used to detect the respiratory phase of patients during the planning and administration of respiratory gated radiotherapy by using four-dimensional computed tomography (4DCT) or 4D positron-emission tomography/CT (4DPET/CT) and the linear accelerator (linac), respectively. Generally, identical respiratory monitoring systems are used for 4DCT, 4DPET/CT, and linac. However, different systems are sometimes used in combination because the accessibility of the respiratory monitoring systems may differ by manufacturer. The combined use of different respiratory monitoring systems in phase-based gating is of concern because the differences in the timing of tags (end-respiration signals algorithmically determined by the respiratory monitoring system), defined by the two systems, may result in phase differences. The purpose of this study is to estimate this difference and evaluate its effect on 4DCT data.
Methods: Ten patients (seven men and three women) with a median age of 75 yr (range: 57–84 yr) were treated by gated stereotactic body radiation therapy between April and December 2009. Two types of respiratory monitoring systems—RPM (Varian Medical Systems) and AZ-733V (Anzai MEDICAL)—were placed on the abdominal surface of the patients, and the respiratory signals were acquired by both systems. The relationship between the amplitude peak and the tag obtained by each respiratory system was analyzed for each patient. Further, the 4DCT images were reconstructed by using the signals obtained from both the RPM and the AZ-733V systems, and the tumor volumes and the tumor centroid positions in the craniocaudal plane were analyzed for each patient.
Results: The correlation factor between the respiratory signals from the RPM system and AZ-733V system was 0.990 (range: 0.940–0.994). The amplitude peak of the RPM system corresponded well with that of the AZ-733V system. The median $\pm$ standard deviation of the phase difference for all the patients ranged from $-4.3 \pm 7.1\%$ to $3.5 \pm 2.2\%$. In the case of some patients, differences were noted between the two systems in the estimation of the tumor centroid position and tumor shape.
Conclusions: The estimation of the position of the tumor centroid and tumor shape may vary with the use of different respiratory monitoring systems. This implies that it is preferable to use the same respiratory monitoring system with 4DCT, 4DPET-CT, and linac. © *2010 American Association of Physicists in Medicine.* [DOI: 10.1118/1.3512798]

Key words: respiratory monitoring system, phase based gating, RGRT, 4DCT

I. INTRODUCTION

Respiratory gated radiotherapy (RGRT) allows irradiation of tumors during phases of the respiratory cycle that involve minimal tumor movement, thus enabling localization of radiation to the tumor.[1–3] RGRT planning is based on the evaluation of tumor motion using four-dimensional com-

puted tomography (4DCT) or 4D positron-emission tomography/CT (4DPET/CT).[4–8]

For respiratory gating, a respiratory monitoring system is used to detect the patient's respiratory phase. The respiratory monitoring systems used for assessing tumor motion during respiration by 4DPET/CT and for gating the linear accelerator (linac) beam generate real-time respiratory signals and end-inspiration signals (tags).[9,10] To date, several respiratory monitoring systems have been developed on the basis of surrogate signals of respiration, such as abdominal displacement, abdominal volume, and pulmonary ventilation.[11–19]

The images acquired by 4DPET/CT are sorted according to the signals generated by the respiratory monitoring system such that they represent individual respiratory phases. These images can be reconstructed on the basis of either the amplitude or the phase of the respiratory signals by using the amplitude-based binning method or phase-based binning method, respectively.[14–16,20–22] The images are then sorted according to the respiratory phase by using a software provided with the CT system. In the amplitude-based respiratory binning method, both the percentile amplitude of the respiratory signal and the direction (inhalation or exhalation) of tidal breathing are used for binning the signals. The CT sinogram file is assigned individualized respiratory percentiles for each amplitude value in the waveform. The phase-based respiratory binning method uses tags that are placed in the CT sinogram file. The tag is placed at the end-inspiration point by the respiratory monitoring system and is determined by algorithm; rarely does the tag correspond exactly with the amplitude peak. The tag is given priority over the actual instant of the maximum end-inspiration point because the respiratory phase is determined in real time.[9,10] The respiratory phases are presented in a scale of 0%–90%, with 0% corresponding to the tag.

The signals generated by the respiratory monitoring system are used for reconstructing the 4DPET/CT images according to the respiratory phases and determining the gating range for the linac. Therefore, ideally, signals from the same respiratory monitoring system should be used with 4DPET/CT and linac. However, some clinics use different respiratory monitoring systems for 4DPET/CT and linac because none of the currently available systems can be connected to both the 4DPET/CT (Biograph, Siemens Medical Solutions, IL) and linac (Trilogy, Varian Medical Systems, Palo Alto, CA). The 4DPET/CT images obtained in this manner cannot be used for treatment planning because of the discrepancies between the results of the two different respiratory monitoring systems. Therefore, RGRT planning is done, wherein images were acquired by a 4DCT scanner (Lightspeed, General Electric Medical Systems, Waukesha, WI) that is connected to the same respiratory monitoring system used for the linac. The purpose of this study is to evaluate the correlation between the signals generated by different respiratory monitoring systems.

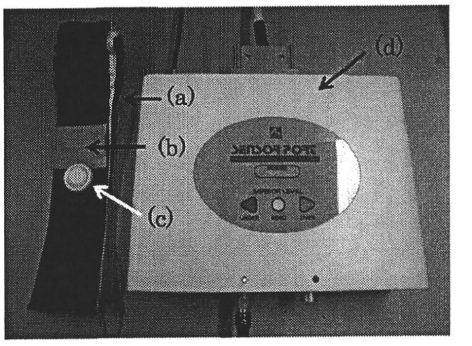

FIG. 1. Photograph showing the components of the AZ-733V system: (a) Belt, (b) pocket for the pressure sensor, (c) pressure sensor, and (d) sensor port.

II. MATERIALS AND METHODS

II.A. Patients

We recruited ten patients (seven male and three female) with a median age of 75 yr (range: 57–84 yr). These patients were treated by gated stereotactic body radiation therapy between April and December 2009. The tumor locations were lung (nine patients) and abdominal lymph nodes (one patient). Written informed consent for data acquisition was obtained from each patient.

II.B. Respiratory monitoring system

In this study, we compared two respiratory monitoring systems: The Real-Time Position Management (RPM) system (version 1.6.5, Varian Medical Systems, Palo Alto, CA) and the AZ-733V system (version. 3.0A, Anzai MEDICAL, Shinagawa, Tokyo).[14,17,19,23]

The RPM system consists of a marker block (with two infrared reflecting dots), an infrared camera, and a control personal computer (PC). The marker block is placed on the abdominal surface of the patient, and the position of the infrared marker is defined on the basis of the images captured by the infrared camera. The system detects the motion of the infrared marker as the respiratory signal, and a tag is computed by a predictive filter in real time. The RPM system frequency is 25 Hz.

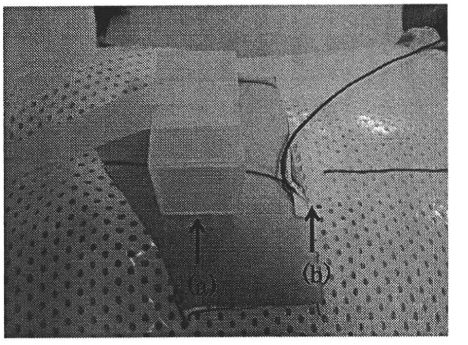

FIG. 2. System setup for the acquisition of two types of respiratory signals. Photograph showing (a) marker block of the RPM system and (b) pressure sensor of the AZ-733V system.

The AZ-733V system consists of a pressure sensor, a belt, a sensor port, and a control personal computer (Fig. 1). The pressure sensor is inserted into the pocket of the belt worn by the patient. The system detects pressure changes, which are considered as the respiratory signals, and the tag is computed by a sweep-point algorithm in real time. The AZ-733V system frequency is 40 Hz.

II.C. Signal acquisition

We acquired signals using both the respiratory monitoring systems, along with the 4DCT data for treatment planning. A single recording was obtained for each patient, and the mean signal acquisition time was 167 s (range: 136–194 s). To fix the patient position during 4DCT data acquisition, we used a body-fixing device (EBS-2000, Engineering System, Matsumoto, Nagano) to immobilize the patients and a body shell (ESFORM, Engineering System, Matsumoto, Nagano) to raise their arms. A part of the body shell in the abdominal region was cut out and removed, and both the respiratory monitoring systems were positioned in this region (Fig. 2). A marker block was placed on the abdomen, at a point between the xiphoid process and umbilicus, and a pressure sensor was inserted between the body shell and the abdomen, near the marker block. The patients were instructed to breathe regularly and freely.

II.D. Signal analysis

The signals from the AZ-733V system were linearly interpolated using the signals from the RPM system because the detection frequencies of the two systems were different. The system times of the two PCs were matched, and the "time stamp" of both systems was used as a benchmark. Using the signals from both respiratory monitoring systems, we analyzed the relationship between the amplitude peak and the tag for each patient. When two amplitude peaks were noted to be adjacent to each other, the amplitude peak nearest to the tag was used for the analysis. The data analysis was performed using a numerical mathematics software (MATLAB, version7, The MathWorks, Inc., Natick, MA). The phase difference was calculated from the time shift of the tag. The definitions of all amplitude peaks and tags generated were as follows (Fig. 3).

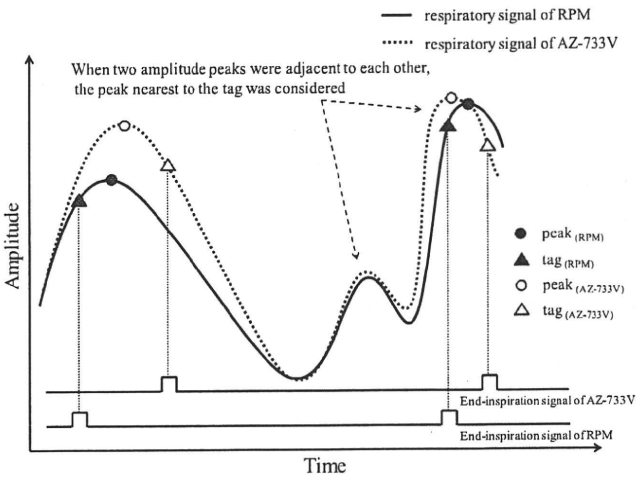

FIG. 3. An illustration showing the amplitude peak and tag. When two amplitude peaks were adjacent to each other, the amplitude peak nearest to the tag was taken into consideration.

- $peak_{(RPM)}$: Point of amplitude peak from the respiratory signal of the RPM system.
- $peak_{(AZ\text{-}733V)}$: Point of amplitude peak from the respiratory signal of the AZ-733V system.
- $tag_{(RPM)}$: Point of end-inspiration by the RPM system as determined by the algorithm.
- $tag_{(AZ\text{-}733V)}$: Point of end-inspiration by the AZ-733V system as determined by the algorithm.

II.E. 4DCT data analysis

From the 4DCT images reconstructed by using signals from both the RPM and the AZ-733V systems, the tumor

TABLE I. Summary of patient characteristics, abdominal displacement (peak-to-peak amplitude), pressure change, and respiratory period for all patients. In the AZ-733V system, we performed gain adjustment, normalized the system to achieve a value of −25–125, and measured the pressure changes. Abbreviations: SD=standard deviation.

				RPM system				AZ-733V system			
				Abdominal displacement (cm)		Breathing period (s)		Pressure change		Breathing period (s)	
Patient No.	Sex	Age	Tumor locations	Median (range)	SD	Median (range)	SD	Median (range)	SD	Median (range)	SD
1	M	57	Left lung S9	2.45 (1.15–2.73)	0.31	5.92 (4.36–6.68)	0.64	73.0 (22.0–102.0)	16.31	5.88 (4.39–6.68)	0.63
2	F	84	Right lung S3	1.60 (1.16–2.13)	0.21	3.12 (2.48–4.00)	0.30	54.5 (28.9–114.0)	18.53	3.13 (2.48–4.00)	0.29
3	M	78	Right lung S1	1.51 (0.60–3.09)	0.63	4.72 (3.79–9.32)	1.01	36.8 (13.0–82.9)	16.67	4.68 (3.76–9.32)	1.01
4	M	75	Right lung S9	1.63 (1.43–2.03)	0.16	4.40 (3.92–6.16)	0.43	98.9 (83.4–135.5)	13.51	4.40 (3.92–6.16)	0.42
5	F	64	Right lung S3	0.96 (0.39–1.50)	0.24	4.32 (3.24–8.12)	0.91	55.8 (22.0–93.0)	15.73	4.44 (3.20–8.12)	0.92
6	M	76	Right lung S2	2.27 (1.71–2.77)	0.21	4.02 (2.56–5.52)	0.60	88.2 (58.6–111.5)	9.97	4.00 (2.56–5.52)	0.60
7	M	81	Left lung S3	1.57 (0.51–1.91)	0.43	6.81 (2.84–12.12)	2.21	91.0 (28.0–113.0)	23.70	6.84 (2.52–12.04)	2.21
8	M	72	Right lung S9	2.16 (1.11–2.96)	0.41	5.36 (4.24–6.80)	0.69	65.0 (28.0–119.0)	17.98	5.42 (4.19–6.64)	0.68
9	F	63	Abdominal LN	1.47 (1.17–1.70)	0.12	5.58 (4.12–11.32)	1.37	87.0 (65.0–105.4)	8.24	5.36 (4.28–11.32)	1.36
10	M	80	Left lung S4	1.00 (0.58–1.41)	0.20	3.36 (2.76–4.08)	0.29	55.0 (27.0–108.0)	20.69	3.40 (2.72–4.08)	0.28

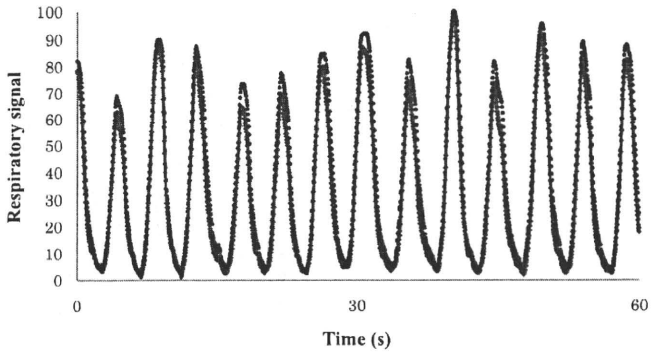

FIG. 4. Correlation between the respiratory signals obtained by the RPM system (solid) and AZ-733V system (interrupted) for patient 2.

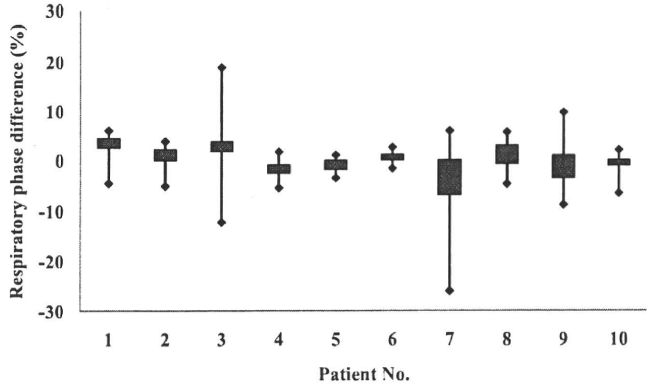

FIG. 5. Box plot showing the differences between the respiratory phases determined by the RPM and AZ-733V systems. The 50% interquartile range and the range of data are displayed. A positive value indicates that the $tag_{(RPM)}$ is sent before the $tag_{(AZ\text{-}733V)}$.

centroid positions in the craniocaudal (CC) direction were analyzed for each patient. The 4DCT data were acquired in the axial cine mode, and the slice thickness was 2.5 mm. The cine duration at each couch position was set to an average breathing period of +2.0 s, and the cine interval between the images was 0.5 s. CT data from both types of scans were reconstructed in a field of view of 500 mm on a 512×512 grid. All CT slices were transferred to a reconstruction workstation (ADVANTAGE 4D workstation, General Electric Medical Systems, Waukesha, WI), and images of each phase were reconstructed by using signals acquired by both the RPM and AZ-733V systems. All phase images were imported into a three-dimensional radiation treatment-planning system (ECLIPSE, version7.5, Varian Medical Systems, Palo Alto, CA). The tumor centroid positions were calculated using ECLIPSE, with the window settings for lung cancer and abdominal lymph node cancer being window widths of 1600 and 400 Hounsfield units (HU) and window levels of −400 and 80 HU, respectively. To eliminate interobserver variations, the target volumes were manually contoured by the same radiation oncologist (with over 10 years of experience), and all contours were reviewed by another radiation oncologist (with over 23 years of experience).

III. RESULTS

III.A. Correlation between the two respiratory monitoring systems

Table I shows the abdominal displacement (peak-to-peak amplitude), pressure change, and breathing period for all patients. Figure 4 compares the respiratory signals recorded by the two respiratory monitoring systems for patient 2. The figure shows that the respiratory signals determined using both systems are similar. The relationship between the time of amplitude peak and tag determined by both systems and the correlation factors between the two types of respiratory signals are summarized in Table II. The correlation factors for the patients were in the range of 0.940–0.994, with a median of 0.990. The time of $peak_{(RPM)}$ corresponds well with that of $peak_{(AZ\text{-}733V)}$ in all cases, except for patients 7 and 9, whose respiration stopped for a long time in the end-inspiration point. The difference in the time of amplitude peak could be attributed to the discrepancy in the pulse rates recorded by the sensors of the two respiratory monitoring systems, which differ in their sensitivity. On the other hand,

TABLE II. The relationship between the amplitude of signals at end-inspiration point (peak) and end-inspiration point determined by the respiratory monitoring system is determined by the algorithm (tag) in both respiratory monitoring systems for all patients. The table shows the variation in the times between the peak and tag. The values are presented as median (minimum-maximum). The table also shows the correlation factors between the two types of respiratory signals.

Patient No.	$t_{peak_{(RPM)}} - t_{peak_{(AZ\text{-}733V)}}$ (s)	$t_{tag_{(RPM)}} - t_{tag_{(AZ\text{-}733V)}}$ (s)	$t_{tag_{(RPM)}} - t_{peak_{(RPM)}}$ (s)	$t_{tag_{(AZ\text{-}733V)}} - t_{peak_{(AZ\text{-}733V)}}$ (s)	RPM vs AZ-733V correlation factor
1	−0.04 (−0.12–0.16)	−0.20 (−0.32–0.24)	−0.16 (−0.28–0.32)	0.04 (−0.04–0.16)	0.966
2	0 (−0.08–0.04)	−0.04 (−0.12–0.16)	0 (−0.08–0.08)	0 (−0.04–0.16)	0.940
3	0 (−0.12–0.16)	−0.16 (−0.28–0.56)	−0.08 (−0.20–0.20)	0.04 (−0.60–0.12)	0.991
4	0.04 (−0.04–0.16)	0.08 (−0.08–0.20)	0.08 (−0.12–0.24)	0.04 (−0.24–0.08)	0.993
5	0 (−0.04–0.08)	0.04 (−0.04–0.16)	0.04 (−0.04–0.16)	0.04 (0.00–0.08)	0.992
6	0.04 (−0.04–0.12)	−0.08 (−0.04–0.08)	−0.08 (−0.16–0.04)	0 (−0.08–0.04)	0.989
7	0.12 (−0.52–0.60)	0.16 (−0.68–2.32)	0.02 (−0.88–0.80)	0.02 (−2.08–0.08)	0.975
8	0.04 (−0.12–0.12)	−0.04 (−0.24–0.28)	−0.04 (−0.32–0.32)	0.04 (−0.44–0.08)	0.991
9	0 (−0.12–0.44)	0.08 (−0.60–0.60)	0 (−0.60–0.64)	0 (−0.60–0.08)	0.994
10	0.04 (−0.04–0.08)	0 (−0.04–0.84)	0 (−0.08–0.80)	0 (−0.12–0.08)	0.958

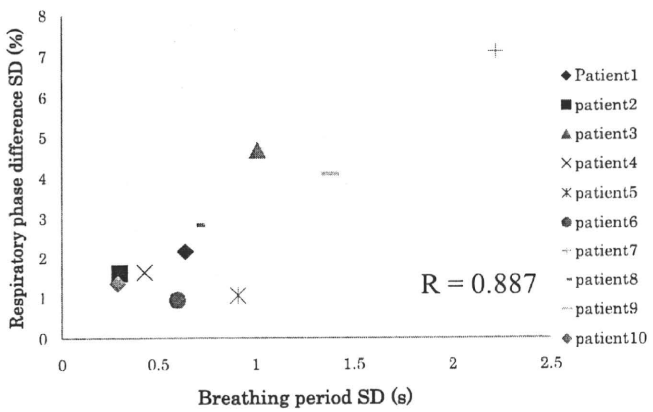

FIG. 6. Respiratory phase difference SD vs breathing period SD for all patients.

a large time lag was observed between $tag_{(RPM)}$ and $tag_{(AZ\text{-}733V)}$. The time lag differed among the patients by a maximum of 2.32 s.

III.B. Respiratory phase difference

The differences between the respiratory phases determined by the RPM and AZ-733V systems are shown in Fig. 5. A positive value indicates that the $tag_{(RPM)}$ was sent before the $tag_{(AZ\text{-}733V)}$. The median ± standard deviation (SD) of phase difference for the patients ranged from $-4.3 \pm 7.1\%$ (range: -26%–5.9%) to $3.5 \pm 2.2\%$ (range: -4.5%–6.0%). The maximum phase difference among all the patients was -26.0%. A comparison of the SDs of the respiratory phase difference data and those of the breathing period data for all the patients gave a correlation factor of 0.887 (Fig. 6). Further, the correlation factor between the SDs of the respiratory phase difference data and those of the abdominal displacement data was 0.584 (Fig. 7). The SDs of abdominal displacement and breathing period were determined using the RPM signals because the data from the AZ-733V system reflects pressure changes only after normalization.

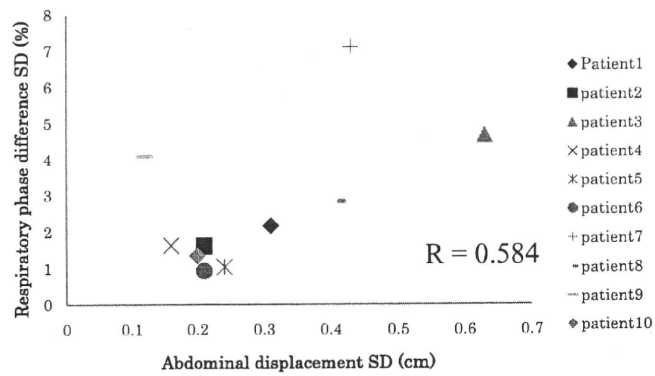

FIG. 7. Respiratory phase difference SD vs abdominal displacement SD for all patients.

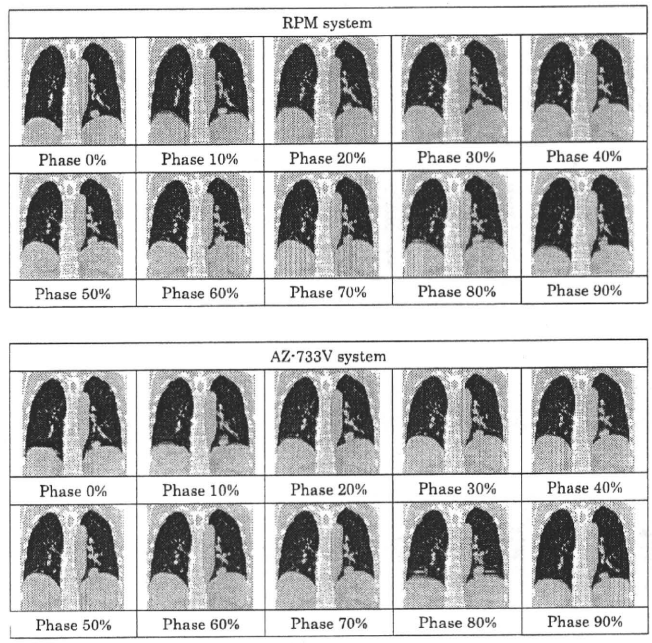

FIG. 8. Coronal sections of the 4DCT images reconstructed by using signals of both the RPM and AZ-733V systems for patient 1.

III.C. Comparison of tumor volume and tumor position obtained by 4DCT

Axial images in all phases reconstructed using the data obtained from the two respiratory monitoring systems for patient 1 are displayed in Fig. 8. The shape of the tumor was different, especially in the 10%, 20%, and 80% phases. Figure 9 shows a comparison of the tumor volume for all patients. The difference between the tumor volume determined by the RPM system and that determined by the AZ-733V system was greater than 25% for some of the phases in a few cases (patients 1, 4, and 9). The maximum volumetric deviation was 47% in the case of patient 4. However, in none of the cases did the tumor volume differ greatly in the end-expiration phase. The tumor volumes in the case of patients 2 and 9 were small, and the tumor in patient 3 was located adjacent to the mediastinum. Therefore, the contour error may influence the change in the tumor volume. Figure 10 shows a comparison of the tumor centroid position in all the patients. In the case of patient 1, the tumor motion determined by the AZ-733V system seems to lead in comparison to that determined using the RPM system. In the case of patients with minimal tumor motion, the estimation of the tumor position and shape did not differ considerably, even when there was a large phase shift.

IV. DISCUSSION

In this study, we compared the respiratory signals and tags acquired using the RPM system to those acquired using the AZ-733V system. To our knowledge, this is the first report that compares the tags determined by two different respiratory monitoring systems.

The respiratory signals were strongly correlated in all the measurements. However, a large phase difference was ob-

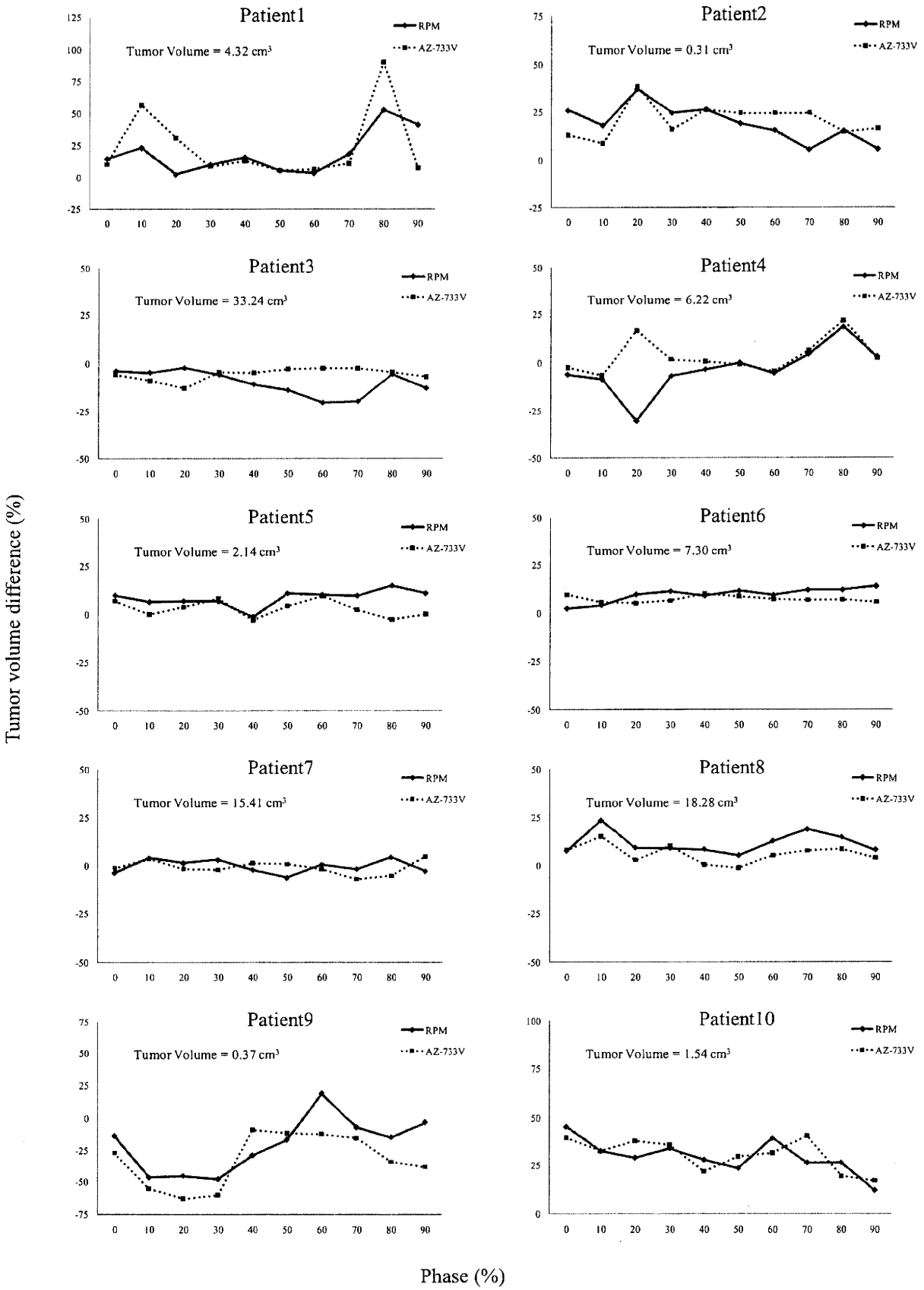

FIG. 9. Comparison of the tumor volume calculated from images reconstructed using the signals acquired by the RPM system (solid) and the AZ-733V system (interrupted) for all patients. The volume of the tumor in each patient that was determined from thin-slice CT images was taken in the breath-holding condition after exhalation and used as a reference tumor volume. A positive value indicates that the tumor volume in each phase image is larger than the tumor volume in the images taken in the breath-holding condition after exhalation.

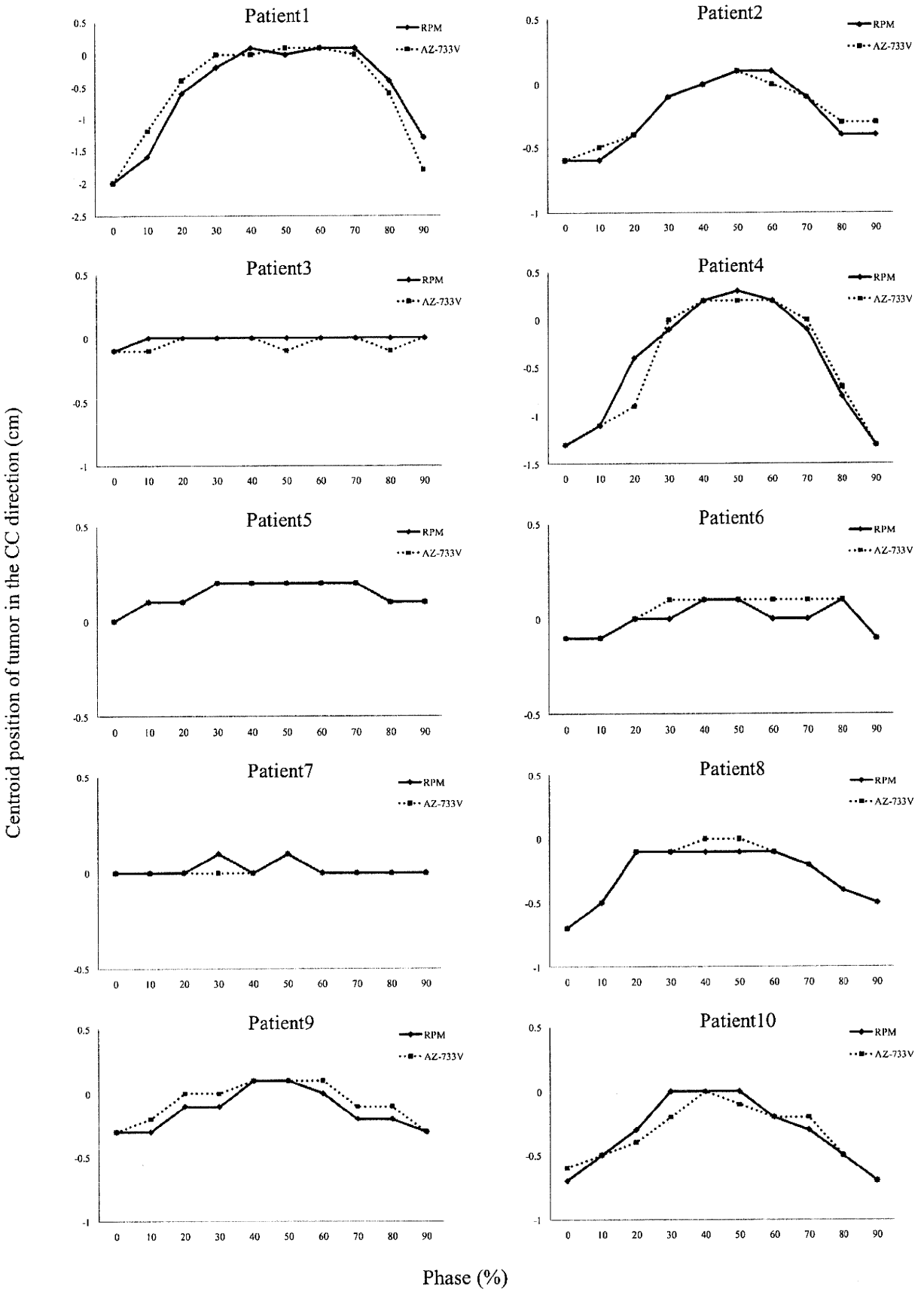

FIG. 10. Comparison of the tumor centroid position in the CC direction determined from images reconstructed using signals acquired by the RPM system (solid) and the AZ-733V system (interrupted) for all patients. The tumor centroid position in the thin-slice CT images was taken in the breath-holding condition after exhalation and used as a reference. A positive value indicates that the tumor centroid in each phase image is located cranial to the tumor centroid position in the images taken in the breath-holding condition after exhalation.

served in the case of several patients. Although the SDs of the phase difference data strongly correlated with those of the breathing period data, they did not correlate with the SDs of the amplitude data. The phase difference during irregular breathing periods can be attributed to the use of different algorithms in the two systems for calculating the tag. This implies that the reproducibility of tag timing cannot be guaranteed when the respiratory monitoring systems used with the 4DPET/CT and the linac are different. When the SD of the breathing period was greater than 1 s, a large phase difference was observed. This implies that the phase difference can be decreased by ensuring the reproducibility and regularity of the breathing period.

Some authors have reported that the SD of the breathing period can be decreased to approximately half the original value—and to less than 1 s in most patients—by coaching the patients.[24–26] Patients can be trained using either audio or visual coaching.[21,24–27] In visual coaching, the breathing pattern is continuously displayed to the patient. In audio coaching, the patient is instructed to breathe in or breathe out at periodic intervals. Kini *et al.*[25] found that visual and audio coaching improved the reproducibility of the amplitude and the breathing periods, respectively. Thus, audio coaching should be used in combination with the RPM and AZ-733V systems for phase-based gating.

Li *et al.*[17] compared the respiratory signals acquired by the RPM and AZ-733V systems that were connected to the 4DCT (Lightspeed, General Electric Medical Systems, Waukesha, WI) and the linac (Primus, Siemens Medical Solutions, IL). Their study involved a phantom experiment, which revealed a strong correlation between the respiratory signals of the two systems (range: 98.2%–99.6%); however, they did not compare the tags recorded for the patients. Hoisak *et al.*[28] compared the respiratory signals obtained using the RPM system and the results of spirometry. The correlation factor varied widely among the patients. Therefore, the use of a combination of respiratory monitoring systems that detect different surrogate signals may lead to a fatal error, even in amplitude-based gating.

The difference in the tumor volumes and centroid positions in each phase image is shown in Figs. 9 and 10, respectively. These results might seem to indicate that the accuracy of expiration phase-based gating achieved by the combined use of the RPM and the AZ-733V systems is identical to that achieved by each system alone. However, a combination of different respiratory monitoring systems must be carefully used because the difference in 4DCT images is only apparent when the shift in tag timing occurs in the couch position where the tumor is included and there is a possibility that the entire effect of the shift in tag timing might not be reflected.

The gating range and internal target volume for planning RGRT are calculated from each phase image. Therefore, the differences in the target defined in each phase image may lead to errors in the estimation of the tumor margin, which may result in the failure of the treatment. Moreover, there may be differences in the respiratory phases determined by the RPM and AZ-733V systems. As shown in Fig. 5, a phase difference of greater than 10% was observed in a few cases (patients 3, 7, and 9). Thus, a 40%–60% gating range in the case of the RPM system may be equivalent to a 30%–50% gating range in the case of the AZ-733V system. For these reasons, it is necessary to evaluate the relationship between the different respiratory monitoring systems used with 4DCT or 4DPET/CT and linac.

V. CONCLUSIONS

We evaluated the respiratory signals and tags defined by two respiratory monitoring systems. The $\text{peak}_{(\text{RPM})}$ corresponded well to the $\text{peak}_{(\text{AZ-733V})}$. However, the points of $\text{tag}_{(\text{RPM})}$ and $\text{tag}_{(\text{AZ-733V})}$ were different in some respiratory patterns, which led to phase differences. Moreover, in the case of some patients, the difference in the tag timing led to a difference in tumor shape and tumor position determined using the 4DCT images because the tag is used as a reference for 4DCT image reconstruction. Therefore, we believe that it would be preferable to use the same respiratory monitoring system with 4DCT, 4DPET-CT, and the linac in RGRT.

[a]Electronic mail: y_otani@saitama-med.ac.jp

[1]S. S. Vedam, V. R. Kini, P. J. Keall, V. Ramakrishnan, H. Mostafavi, and R. Mohan, "Quantifying the predictability of diaphragm motion during respiration with a noninvasive external marker," Med. Phys. **30**, 505–513 (2003).

[2]H. A. Shih, S. B. Jiang, K. M. Aljarrah, K. P. Doppke, and N. C. Choi, "Internal target volume determined with expansion margins beyond composite gross tumor volume in three-dimensional conformal radiotherapy for lung cancer," Int. J. Radiat. Oncol., Biol., Phys. **60**, 613–622 (2004).

[3]C. Nelson, G. Starkschall, P. Balter, R. C. Morice, C. W. Stevens, and J. Y. Chang, "Assessment of lung tumor motion and setup uncertainties using implanted fiducials," Int. J. Radiat. Oncol., Biol., Phys. **67**, 915–923 (2007).

[4]P. Keall, "4-dimensional computed tomography imaging and treatment planning," Semin. Radiat. Oncol. **14**, 81–90 (2004).

[5]R. W. Underberg, F. J. Lagerwaard, J. P. Cuijpers, B. J. Slotman, J. R. van Sörnsen de Koste, and S. Senan, "Four-dimensional CT scans for treatment planning in stereotactic radiotherapy for stage I lung cancer," Int. J. Radiat. Oncol., Biol., Phys. **60**, 1283–1290 (2004).

[6]S. Senan, D. De Ruysscher, P. Giraud, R. Mirimanoff, and V. Budach, "Literature-based recommendations for treatment planning and execution in high-dose radiotherapy for lung cancer," Radiother. Oncol. **71**, 139–146 (2004).

[7]E. Brianzoni, G. Rossi, S. Ancidei, A. Berbellini, F. Capoccetti, C. Cidda, P. D'Avenia, S. Fattori, G. C. Montini, G. Valentini, A. Proietti, and C. Algranati, "Radiotherapy planning: PET/CT scanner performances in the definition of gross tumour volume and clinical target volume," Eur. J. Nucl. Med. Mol. Imaging **32**, 1392–1399 (2005).

[8]D. De Ruysscher, S. Wanders, A. Minken, A. Lumens, J. Schiffelers, C. Stultiens, S. Halders, L. Boersma, A. Baardwijk, T. Verschueren, M. Hochstenbag, G. Snoep, B. Wouters, S. Nijsten, S. M. Bentzen, M. Kroonenburgh, M. Ollers, and P. Lambin, "Effects of radiotherapy planning with a dedicated combined PET-CT-simulator of patients with non-small cell lung cancer on dose limiting normal tissues and radiation dose escalation: A planning study," Radiother. Oncol. **77**, 5–10 (2005).

[9]M. J. Fitzpatrick, G. Starkschall, J. A. Antolak, J. Fu, H. Shukla, P. J. Keall, P. Klahr, and R. Mohan, "Displacement-based binning of time-dependent computed tomography image data sets," Med. Phys. **33**, 235–246 (2006).

[10]J. R. Olsen, W. Lu, J. P. Hubenschmidt, M. M. Nystrom, P. Klahr, J. D. Bradley, D. A. Low, and P. J. Parikh, "Effect of novel amplitude/phase binning algorithm on commercial four-dimensional computed tomography quality," Int. J. Radiat. Oncol., Biol., Phys. **70**, 243–252 (2008).

[11]T. Zhang, H. Keller, M. J. O'Brien, T. R. Mackie, and B. Paliwal, "Application of the spirometer in respiratory gated radiotherapy," Med. Phys. **30**, 3165–3171 (2003).

[12]E. C. Ford, G. S. Mageras, E. Yorke, and C. C. Ling, "Respiration corre-

lated spiral CT: A method of measuring respiratory-induced anatomic motion for radiation treatment planning," Med. Phys. **30**, 88–97 (2003).
[13]Y. Tsunashima, T. Sakae, Y. Shioyama, K. Kagei, T. Terunuma, A. Nohtomi, and Y. Akine, "Correlation between the respiratory waveform measured using a respiratory sensor and 3D tumor motion in gated radiotherapy," Int. J. Radiat. Oncol., Biol., Phys. **60**, 951–958 (2004).
[14]R. I. Berbeco, S. Nishioka, H. Shirato, G. T. Chen, and S. B. Jiang, "Residual motion of lung tumours in gated radiotherapy with external respiratory surrogates," Phys. Med. Biol. **50**, 3655–3667 (2005).
[15]R. I. Berbeco, S. Nishioka, H. Shirato, and S. B. Jiang, "Residual motion of lung tumors in end-of-inhale respiratory gated radiotherapy based on external surrogates," Med. Phys. **33**, 4149–4156 (2006).
[16]W. Lu, P. J. Parikh, J. P. Hubenschmidt, J. D. Bradley, and D. A. Low, "A comparison between amplitude sorting and phase-angle sorting using external respiratory measurement for 4D CT," Med. Phys. **33**, 2964–2974 (2006).
[17]X. A. Li, C. Stepaniak, and E. Gore, "Technical and dosimetric aspects of respiratory gating using a pressure-sensor motion monitoring system," Med. Phys. **33**, 145–154 (2006).
[18]B. Cho, Y. Suh, S. Dieterich, and P. J. Keall, "A monoscopic method for real-time tumour tracking using combined occasional x-ray imaging and continuous respiratory monitoring," Phys. Med. Biol. **53**, 2837–2855 (2008).
[19]K. Weibert, S. Biller, T. G. Wendt, and T. Wiezorek, "Dosimetry of a linear accelerator under respiratory gating," Z. Med. Phys. **19**, 136–141 (2009).
[20]S. S. Vedam, P. J. Keall, V. R. Kini, and R. Mohan, "Determining parameters for respiration-gated radiotherapy," Med. Phys. **28**, 2139–2146 (2001).
[21]R. George, T. D. Chung, S. S. Vedam, V. Ramakrishnan, R. Mohan, E. Weiss, and P. J. Keall, "Audio-visual biofeedback for respiratory-gated radiotherapy: Impact of audio instruction and audio-visual biofeedback on respiratory-gated radiotherapy," Int. J. Radiat. Oncol., Biol., Phys. **65**, 924–933 (2006).
[22]U. W. Langner and P. J. Keall, "Accuracy in the localization of thoracic and abdominal tumors using respiratory displacement, velocity, and phase," Med. Phys. **36**, 386–393 (2009).
[23]S. A. Nehmeh, Y. E. Erdi, T. Pan, E. Yorke, G. S. Mageras, K. E. Rosenzweig, H. Schoder, H. Mostafavi, O. Squire, A. Pevsner, S. M. Larson, and J. L. Humm, "Quantitation of respiratory motion during 4D-PET/CT acquisition," Med. Phys. **31**, 1333–1338 (2004).
[24]G. S. Mageras, E. Yorke, K. Rosenzweig, L. Braban, E. Keatley, E. Ford, S. A. Leibel, and C. C. Ling, "Fluoroscopic evaluation of diaphragmatic motion reduction with a respiratory gated radiotherapy system," J. Appl. Clin. Med. Phys. **2**, 191–200 (2001).
[25]V. R. Kini, S. S. Vedam, P. J. Keall, S. Patil, C. Chen, and R. Mohan, "Patient training in respiratory-gated radiotherapy," Med. Dosim. **28**, 7–11 (2003).
[26]S. Lim, S. H. Park, S. D. Ahn, Y. Suh, S. S. Shin, S. W. Lee, J. H. Kim, E. K. Choi, B. Y. Yi, S. I. Kwon, S. Kim, and T. S. Jeung, "Guiding curve based on the normal breathing as monitored by thermocouple for regular breathing," Med. Phys. **34**, 4514–4518 (2007).
[27]M. Nakamura, Y. Narita, Y. Matsuo, M. Narabayashi, M. Nakata, A. Sawada, T. Mizowaki, Y. Nagata, and M. Hiraoka, "Effect of audio coaching on correlation of abdominal displacement with lung tumor motion," Int. J. Radiat. Oncol., Biol., Phys. **75**, 558–563 (2009).
[28]J. D. Hoisak, K. E. Sixel, R. Tirona, P. C. Cheung, and J. P. Pignol, "Correlation of lung tumor motion with external surrogate indicators of respiration," Int. J. Radiat. Oncol., Biol., Phys. **60**, 1298–1306 (2004).

Esophagus (2010) 7:7–22
DOI 10.1007/s10388-010-0228-6

SPECIAL ARTICLE

Soji Ozawa · Yuji Tachimori · Hideo Baba
Hisahiro Matsubara · Kei Muro · Hodaka Numasaki
Tsuneo Oyama · Masayuki Shinoda · Hiroya Takeuchi
Otsuo Tanaka · Teruki Teshima · Harushi Udagawa
Takashi Uno · J. Patrick Barron

Comprehensive Registry of Esophageal Cancer in Japan, 2002

Preface

We are very pleased to publish the Comprehensive Registry of Esophageal Cancer in Japan, 2002, we thank all the members of the Japan Esophageal Society who made great contributions in preparing this material.

First of all, we describe the history of the registry of esophageal cancer cases in Japan. The Registration Committee for Esophageal Cancer of the Japan Esophageal Society, has registered cases of esophageal cancer since 1976 and published the first issue of the Comprehensive Registry of Esophageal Cancer in Japan in 1979. The Act for the Protection of Personal Information was promulgated in 2003, and began to be enforced in 2005. The purpose of this Act is to protect the rights and interests of individuals while taking into consideration the usefulness of personal information, keeping in mind the remarkable increase in the use of personal information arising from the development of today's advanced information and communications society. The registry of esophageal cancer cases has required some improvements to comply with the Acts. The new registration system has been considered for several years and was finally completed in 2008. The most important point was "anonymity in an unlinkable fashion" using encryption with a "hash function". Finally, the registry resumed registering cases of esophageal cancer that had been treated in 2001.

We briefly summarized the Comprehensive Registry of Esophageal Cancer in Japan, 2002. A total of 4281 cases were registered from 222 institutions in Japan. As for the histologic type of cancer according to biopsy specimens, squamous cell carcinoma and adenocarcinoma accounted for 92.9% and 2.4%, respectively. Regarding clinical results, the 5-year survival rates of patients treated using endoscopic mucosal resection, concurrent chemoradiotherapy, radiotherapy alone, chemotherapy alone, or esophagectomy were 87.7%, 22.9%, 15.1%, 1.7%, and 44.1%, respectively. Concerning the approach used to perform an esophagectomy, 16.5% of the cases were performed endoscopically, that is, thoracoscopically, laparoscopically, or mediastinoscopically. Regarding the reconstruction route, the retrosternal, the posterior mediastinal and the intrathoracic route were used in 35.4%, 32.4% and 17.9% of cases, respectively. The percentage of operative deaths occurring within 30 days or less after operation and the percentage of postoperative hospital deaths occurring 31 days or more after operation were 1.2% (25 out of 2028 cases) and 2.0% (41 out of 2028 cases), respectively.

We hope that this Comprehensive Registry of Esophageal Cancer in Japan for 2002 helps to improve all aspects of the diagnosis and treatment of esophageal cancer.

These data were first issued on 1 March, 2010, as the *Comprehensive Registry of Esophageal Cancer in Japan, 2002*. Not all pages are reprinted here; however, the original table and figure numbers have been kept. The authors were at the time members of the Registration Committee for Esophageal Cancer, the Japan Esophageal Society, and made great contributions in preparing this material.

Japan Esophageal Society, Sun-city Inohana B, 3-2-4 Inohana, Chuo-ku, Chiba 260-0856, Japan
Tel./Fax +81-43-222-5665

Contents

Reference
N-category in: The Japanese Classification of Esophageal Cancer, 9th edition, Japan Esophageal Society

I. Clinical factors of esophageal cancer patients treated in 2002

1. Institution-registered cases in 2002

Institutions	Institutions
Aichi Cancer Center	Kikuna Memorial Hospital
Aizawa Hospital	Kin-ikyo Chuo Hospital
Akita University Hospital	Kinki Central Hospital
Asahikawa Medical College Hospital	Kinki University Hospital
Chiba Cancer Center	Kinki University Nara Hospital
Chiba Prefecture Sawara Hospital	Kiryu Kosei General Hospital
Chiba University Hospital	Kitakyushu Municipal Medical Center
Chubu Rosai Hospital	Kitasato University Hospital
Dokkyo Medical University Hospital	Kobe City Medical Center General Hospital
Foundation for Detection of Early Gastric Carcinoma	Kobe University Hospital
Fuchu Hospital	Kumamoto University Hospital
Fujioka General Hospital	Kurume Daiichi Social Insurance Hospital
Fujita Health University	Kurume University Hospital
Fujita Health University Banbuntane Hotokukai Hospital	Kuwana City Hospital
Fukaya Red Cross Hospital	Kyorin University Hospital
Fukaya University Chikushi Hospital	Kyoto Daini Sekijuji Hospital
Fukuoka University Hospital	Kyoto University Hospital
Fukuyama Hospital	Kyushu Central Hospital
Gunma Central General Hospital	Kyushu University Hospital
Gunma Prefecture Cancer Center	Kyushu University Hospital at Beppu
Gunma University Hospital	Matsuda Hospital
Hachinohe City Hospital	Matsudo City Hospital
Hachioji Digestive Disease Hospital	Matsushita Memorial Hospital
Hakodate Goryokaku Hospital	Matsuyama Red Cross Hospital
Hamamatsu University School of Medicine, University Hospital	Mie University Hospital
Hannan Chuo Hospital	Mito Red Cross Hoapital
Health Insurance Naruto Hospital	Miyazaki Social Insurance Hospital
Hiratsuka City Hospital	Murakami General Hospital
Hiratsuka Kyosai Hospital	Mutsu General Hospital
Hiroshima City Asa Hospital	Nagahama City Hospital
Hiroshima University Research Institute for Radiation Biology Medicine	Nagano Prefectual Kiso Hospital
Hofu Institute of Gastroenterology	Nagano Red Cross Hospital
Hokkaido University Hospital	Nagaoka Chuo General Hospital
Hyogo Prefectural Nishinomiya Hospital	Nagasaki University Hospital
Ida Municipal Hospital	Nagayoshi General Hospital
Imazato Icho Hospital	Nagoya City University Hospital
International University of Health and Welfare Mita Hospital	Nagoya Daiichi Red Cross Hospital
Isehara Cooperation Hospital	Nagoya Tokushukai General Hospital
Ishikawa Kenritsu Chuo Hospital	Nagoya University Hospital
Ishinomaki Red Cross Hospital	Nanpuh Hospital
Iwakuni Clinical Center	Nara Medical University Hospital
Iwakuni Medical Center	National Cancer Center Hospital
Iwate Medical University Hospital	National Cancer Center Hospital East
Iwate Prefecture Kitagami Hospital	National Defense Medical College Hospital
JFE Kenpo Kawatetsu Chiba Hospital	National Hospital Organization Chiba Medical Center
Jichi Medical University Hospital	National Hospital Organization Hakodate Hospital
Jikei University Hospital	National Hospital Organization Kanmon Medical Center
Juntendo University Hospital	National Hospital Organization Kasumigaura Medical Center
Juntendo University Shizuoka Hospital	National Hospital Organization Kyushu Cancer Center
Kagawa Prefectual Central Hospital	National Hospital Organization Matsumoto National Hospital
Kagoshima Kenritsu Satsunan Hospital	National Hospital Organization Nagano Medical Center
Kagoshima University Hospital	National Hospital Organization Nagasaki Medical Denter
Kanagawa Cancer Center	National Hospital Organization Osaka Natitional Hospital
Kanazawa University Hospital	National Hospital Organization Tochigi National Hospital
Kansai Rosai Hospital	National Hospital Organization Tokyo Medical Center
Kashima Rosai Hospital	Nihon University Itabashi Hospital
Kawasaki Medical School Hospital	Nihonkai Genaral Hospital
Kawasaki Municipal Hospital	Niigata Cancer Center Hospital
Keio University Hospital	Niigata City General Hospital
Keiyukai Sapporo Hospital	Niigata Prefectural Shibata Hospital

Institutions	Institutions
Niigata University Medical and Dental Hospital Nikko Memorial Hospital Nippon Medical School Chiba Hokusoh Hospital Nippon Medical School Hospital Nippon Medical School Musashi Kosugi Hospital Nippon Medical School Tama Nagayama Hospital Nishi-Kobe Medical Center Nishinomiya Municipal Central Hospital Nomura Hospital NTT East Japan Kanto Hospital NTT West Osaka Hospital Numazu City Hospital Obihiro Kosei Hospital Ohta General Hospital Foundation Ohta Nishinouchi Hospital Oita Red Cross Hospital Okayama Saiseikai General Hospital Okayama University Hospital Onomichi Municipal Hospital Osaka Koseinenkin Hospital Osaka Medical Center for Cancer and Cardiovascular Diseases Osaka Medical College Hospital Osaka Prefectural Hospital Organization Osaka General Medical Center Osaka Senin Hoken Hospital Osaka University Hospital Otsu Red Cross Hospital Rinku General Medical Center City Izumisano Hospital Saiseikai Fukushima General Hospital Saiseikai Gose Hospital Saiseikai Hiroshima Hospital Saiseikai Maebashi Hospital Saiseikai Narashino Hospital Saiseikai Omura Hospital Saitama City Hospital Saitama Medical Center Saitama Medical Center Jichi Medical University Saitama Medical University Hospital Saitama Medical University International Medical Center Saitama Red Cross Hospital Saitama Social Insurance Hospital Sakai Municipal Hospital Saku Central Hospital Sanno Hospital Seifukai Rakusei Hospital Seirojika National Hospital University Hospital Sendai City Hospital Sendai Medical Center Shiga University of Medical Science Hospital Shikoku Cancer Center Shimane University Hospital Shimura Hospital Shinshiro Municipal Hospital Shinshu University Hospital Shizuoka City Shizuoka Hospital Shouzankai Saiki Hospital Showa Inan General Hospital Showa University Fujigaoka Hospital Showa University Hospital Social Insurance Omuta Tenryo Hospital Social Insurance Tagawa Hospital Social Insurance Yokohama Central Hospital	Sonoda Daiichi Hospital Southern Region Hospital St.Therese Hospital Sugita Genpaku Memorial Obama Municipal Hospital Suita Municipal Hospital Showa University Toyosu Hospital Tachikawa Hospital Takaoka Hospital Takasago Municipal Hospital Teikyo University School of Medicine Hospital, Mizonokuchi Toho University Omori Medical Center Tohoku Kosai Hospital Tohoku University Hospital Tokai University Hospital Tokai University Tokyo Hospital Tokushima University Hospital Tokyo Dental College Ichikawa General Hospital Tokyo Medical and Dental University Hospital Tokyo Medical University Kasumigaura Hospital Tokyo Metropolitan Cancer and Infectious Center Komagome Hospital Tokyo Women's Medical University Hospital Tokyo Women's Medical University Medical Center East Toranomon Hospital Tottori Prefectural Central Hospital Tottori University Hospital Toyama Hospital, International Medical Center of Japan Toyama Prefectual Central Hospital Toyama University Hospital Tsuchiura Kyodo Hospital Tsukuba University Hospital University of Fukui Hospital University of the Ryukyu Hospital Wakayama Medical University Hospital Yamagata Prefectural Central Hospital Yamagata University Hospital Yamaguchi University Hospital Yamanashi Prefectural Central Hospital Yamanashi University Hospital Yao Municipal Hospital Yokohama City University Yokohama City University Medical Hospital Yuri General Hospital

(Total 222 institutions)

2. Patient Background

Table 1 Age and gender

*** Excluding 9 cases of unknown gender**

Age	Male	Female	Unknown	Cases (%)
~29	2	0	0	2 (0.0%)
30~39	13	0	0	13 (0.3%)
40~49	126	31	0	157 (3.7%)
50~59	833	126	0	959 (22.6%)
60~69	1372	191	0	1563 (36.9%)
70~79	1141	173	0	1314 (31.0%)
80~89	161	47	0	208 (4.9%)
90~	13	6	0	19 (0.4%)
Total	3661	574	0	4235
Missing	29	8	0	37

A missing case was defined as a case in which no option was selected.

An unknown case was defined as a case in which the "Unknown" option was selected.

Table 12 Tumor location

*** Excluding 440 treatment unknown, missing cases concerning treatment type**

Location of tumor	Endoscopic treatment (%)	Chemotherapy and/or radiotherapy (%)	Surgery		Total (%)
			Palliative operation (%)	Esophagectomy (%)	
Cervical	7 (1.6%)	82 (6.5%)	1 (1.1%)	62 (3.1%)	152 (4.0%)
Upper thoracic	60 (13.3%)	207 (16.4%)	17 (19.1%)	225 (11.2%)	509 (13.4%)
Middle thoracic	264 (58.7%)	645 (51.1%)	40 (44.9%)	1019 (50.7%)	1968 (51.6%)
Lower thoracic	85 (18.9%)	276 (21.9%)	25 (28.1%)	536 (26.7%)	922 (24.2%)
Abdominal	13 (2.9%)	27 (2.1%)	4 (4.5%)	126 (6.3%)	170 (4.5%)
EG	1 (0.2%)	0	2 (2.2%)	12 (0.6%)	15 (0.4%)
EG-Junction(E=G)	2 (0.4%)	3 (0.2%)	0	13 (0.6%)	18 (0.5%)
Cardia (G)	1 (0.2%)	1 (0.1%)	0	3 (0.1%)	5 (0.1%)
Others	0	0	0	0	0
Unknown	17 (3.8%)	21 (1.7%)	0	14 (0.7%)	52 (1.4%)
Total	450	1262	89	2010	3811
Missing	4	2	0	9	15

EG: esophagogastric

Table 15 Histologic types of cancer according to biopsy specimens

*** Excluding 440 treatment unknown, missing cases concerning treatment type**

Histologic types	Endoscopic treatment (%)	Chemotherapy and/or radiotherapy (%)	Surgery		Total (%)
			Palliative operation (%)	Esophagectomy (%)	
Not examined	13 (2.9%)	9 (0.7%)	0	10 (0.5%)	32 (0.8%)
SCC	403 (90.2%)	1186 (94.0%)	83 (93.3%)	1862 (92.7%)	3534 (92.9%)
SCC	300 (67.1%)	640 (50.7%)	41 (46.1%)	1005 (50.0%)	1986 (52.2%)
Well diff.	23 (5.1%)	70 (5.5%)	5 (5.6%)	195 (9.7%)	293 (7.7%)
Moderately diff.	66 (14.8%)	307 (24.3%)	30 (33.7%)	494 (24.6%)	897 (23.6%)
Poorly diff.	14 (3.1%)	169 (13.4%)	7 (7.9%)	168 (8.4%)	358 (9.4%)
Adenocarcinoma	16 (3.6%)	15 (1.2%)	3 (3.4%)	57 (2.8%)	91 (2.4%)
Undifferentiated	2 (0.4%)	15 (1.2%)	0	10 (0.5%)	27 (0.7%)
Carcinosarcoma	0	5 (0.4%)	0	9 (0.4%)	14 (0.4%)
Malignant melanoma	0	1 (0.1%)	0	5 (0.2%)	6 (0.2%)
Other tumors	2 (0.4%)	7 (0.6%)	1 (1.1%)	17 (0.8%)	27 (0.7%)
Dysplasia	0	0	0	0	0
Unknown	11 (2.5%)	24 (1.9%)	2 (2.2%)	38 (1.9%)	75 (2.0%)
Total	447	1262	89	2008	3806
Missing	9	6	0	20	35

SCC: squamous cell carcinoma

Table 19 Organs with metastasis in cM1 case (clinical TNM-classification)

*** Excluding 440 treatment unknown, missing cases concerning treatment type**

Metastatic organs	Endoscopic treatment (%)		Chemotherapy and/or radiotherapy (%)		Surgery				Total (%)	
					Palliative operation (%)		Esophagectomy (%)			
PUL	7	(35.0%)	75	(20.5%)	1	(14.3%)	11	(6.9%)	94	(17.0%)
OSS	1	(5.0%)	13	(3.6%)	0		0		14	(2.5%)
HEP	5	(25.0%)	76	(20.8%)	3	(42.9%)	11	(6.9%)	95	(17.2%)
BRA	1	(5.0%)	7	(1.9%)	0		1	(0.6%)	9	(1.6%)
LYM	5	(25.0%)	166	(45.4%)	2	(28.6%)	126	(78.8%)	299	(54.1%)
MAR	0		0		1	(14.3%)	0		1	(0.2%)
PLE	0		4	(1.1%)	0		0		4	(0.7%)
PER	0		3	(0.8%)	0		1	(0.6%)	4	(0.7%)
SKI	0		5	(1.4%)	0		5	(3.1%)	10	(1.8%)
OTH	1	(5.0%)	15	(4.1%)	0		3	(1.9%)	19	(3.4%)
Unknown	0		2	(0.5%)	0		2	(1.3%)	4	(0.7%)
Lesions	20		366		7		160		553	
Missing	3		54		1		5		63	
One organ	11	(73.3%)	270	(85.7%)	5	(83.3%)	154	(97.5%)	440	(89.1%)
Two organs	3	(20.0%)	36	(11.4%)	1	(16.7%)	2	(1.3%)	42	(8.5%)
Three organs	1	(6.7%)	6	(1.9%)	0		0		7	(1.4%)
Four organs~	0		1	(0.3%)	0		0		1	(0.2%)
Unknown	0		2	(0.6%)	0		2	(1.3%)	4	(0.8%)
Total cases	15		315		6		158		494	
Missing	3		54		1		5		63	

PUL: lung, OSS: bone, HEP: liver, BRA: brain, LYM: lymph node, MAR: marrow,

PLE: pleural membrane, PER:peritoneal membrane, SKI: skin, OTH: others

Table 20 Clinical Stage (clinical TNM-classification)

*** Excluding 440 treatment unknown, missing cases of concerning treatment type**

cStage	Endoscopic treatment (%)		Chemotherapy and/or radiotherapy (%)		Surgery				Total (%)	
					Palliative operation (%)		Esophagectomy (%)			
0	84	(18.7%)	4	(0.3%)	1	(1.1%)	14	(0.7%)	103	(2.7%)
I	292	(65.0%)	149	(11.8%)	11	(12.4%)	473	(23.5%)	925	(24.3%)
IIA	2	(0.4%)	125	(9.9%)	19	(21.3%)	388	(19.3%)	534	(14.0%)
IIB	2	(0.4%)	78	(6.2%)	7	(7.9%)	281	(14.0%)	368	(9.7%)
III	21	(4.7%)	450	(35.7%)	38	(42.7%)	654	(32.5%)	1163	(30.5%)
IV	0		79	(6.3%)	2	(2.2%)	27	(1.3%)	108	(2.8%)
IVA	6	(1.3%)	70	(5.6%)	1	(1.1%)	76	(3.8%)	153	(4.0%)
IVB	10	(2.2%)	196	(15.6%)	4	(4.5%)	53	(2.6%)	263	(6.9%)
Unknown	32	(7.1%)	109	(8.7%)	6	(6.7%)	44	(2.2%)	191	(5.0%)
Total	449		1260		89		2010		3808	
Missing	7		8		0		18		33	